WILEY-VCH

A Semi-Liquid Electrode toward Stable Zn Powder Anode

*Qun Liu, Zhenlu Yu, Rui Zhou, Biao Zhang**

Department of Applied Physics, The Hong Kong Polytechnic University, Hung Hom, Hong Kong, China. E-mail: biao.ap.zhang@polyu.edu.hk

Abstract

Zn powder anode possesses great versatility compared to the Zn foil counterpart, but the rough surface with a high surface area aggravates the corrosion and dendrite growth. Herein, a dendrite-free and anti-corrosive semi-liquid Zn anode (SLA) is successfully fabricated based on Zn powder and a thickening agent. Benefiting from the rheological property, the unique anode effectively releases the stress induced by Zn plating, especially under high current densities. Meanwhile, the dual-conductive, i.e., ionic and electronic, medium homogenizes the ion flux and allows the stripping/plating to occur within the entire anode. In a symmetric cell, the SLA anode exhibits stable electrochemical behavior with a prolonged lifespan at the current rate of 5 mA cm^{-2}/10 mA cm^{-2} under the capacity of 5 mAh cm^{-2}/10 mAh cm^{-2}. Improved durability of more than 5000 cycles is endowed when assembling an SLA anode with a vanadium-based cathode. This work provides an electrode rheology-based approach to overcome the stability challenge of powder anode for scale-up manufacturing.

Keywords: Semi-liquid electrode, Zn powder, stress relaxation, rheological property, anti-corrosion

1. Introduction

As a promising green energy system, aqueous zinc-ion batteries offer advantages in cost and safety, benefiting from neutral or slightly acidic aqueous electrolytes.[1] However, conventional Zn metal, the most popular anode for zinc-ion batteries, suffers from severe corrosion and uncontrolled dendrite evolution during stripping/plating process, leading to short

circuits and a sharp decline in lifespan.[2] The situation becomes more aggravated in Zn powder-based electrodes than in Zn foil counterparts due to the former's high surface area and rough morphology. Although most works adopt Zn metal foil anode, the Zn powder shows superior versatility for industry application.[3]

Some novel strategies have been proposed to suppress dendrite growth by regulating Zn deposition behavior, including engineering the three-dimensional host, using electrolyte additives and high-concentration electrolytes, constructing artificial interfaces, and modifying separators.[4] Nevertheless, most of these methods succeed primarily in Zn foil anodes with dendrite inhibition through external physical and chemical treatment rather than eliminating the dendrite formation from the source. Alternatively, the stress-release mechanism has been proved as a fundamental way to circumvent dendrite formation.[5] For instance, soft substrate-based materials will produce wrinkles to avoid stress concentration once they destabilize under compressed stress from electrochemical deposition.[6] However, the detachment occurs between soft substrate and newly deposited metal because of the mechanical mismatch under repeated stripping/plating process. To mitigate the problems of soft substrate, liquid metal anodes are considered potential candidates. For example, the customized Zn-rich liquid metal (ZnGaIn) effectively enables stress relaxation of plated Zn metal, inducing the dendrite-free morphology.[7] Unfavorably, the high cost and limited options of liquid metal rule it out for a universal application in large energy storage systems.[8]

Semi-liquid material is a non-Newtonian fluid resulting from directly mixing two phases of matter with specific content, like metal particles and liquid.[9] Such homogeneous colloidal dispersion exhibits fluidity upon vibration and liquid-like rheological (shear-thinning) properties. Under external force, semi-liquid material will lose strength to release the deposition stress. Thus, the semi-liquid anode is expected to deliver dendrite-free plating behavior similar to the function of liquid metal. Most importantly, the strategy is fully compatible with Zn power.

Therefore, we design a semi-liquid anode (denoted as SLA) by mixing Zn powder with a dual-conductive (ionically and electronically) poly(ethylene glycol) (PEG)-Zn^{2+}/carbon composite matrix. The dominant features of SLA consist of the following aspects: i) The SLA exhibits rheological properties with the shear strain, effectively eliminating the stress and inducing dendrite-free Zn deposition; ii) dual-conductive network homogenizes the Zn^{2+} flux and induces the stripping/plating to take place within the entire volume of the electrode; iii) PEG in SLA enables anti-corrosive characteristics; iv) facile fabricating techniques and cost-effective raw materials are conducive to scale-up application. Owing to the extended attributes of the SLA, the symmetric cell with SLA delivers an improved lifespan of more than 450 h under 5 mA cm^{-2} for 5 mAh cm^{-2} and 100 h under 10 mA cm^{-2} for 10 mAh cm^{-2}, achieving one of the highest cumulative capacities compared with reported synthetic Zn anodes. In addition, SLA contributes to the enhancement of vanadium-based full cells, whereas long-term stability with over 5000 cycles is realized.

2. Results and Discussions

The synthetic procedure for SLA is schematically illustrated in **Figure S1**. Specifically, commercial Zn microparticles (**Figure S2**) and super P were added into poly(ethylene glycol) (PEG, MW=400) containing zinc perchlorate hexahydrate (mass ratio=2:1). The mixture was ground to form a homogeneous colloidal dispersion and subsequently coated on stainless steel for SLA formation. Solid Zn powder anode and Zn foil were studied as contrast samples. The solid Zn powder anode was prepared by the slurry-coating method described in the experimental section, while Zn foil with a thickness of 100 μm was selected. Unlike solid anode, a significant feature of SLA is the dual-conductive medium, where PEG/Zn^{2+} provides ion conductive paths and super P constructs the electron transfer framework. According to the electrochemical impedance spectroscopy (EIS) and I-t result (**Figure S3-S4**), the ionic and electronic conductivity are 12.6 mS m^{-1} and 6.5 mS m^{-1}, respectively. As demonstrated in

Figure 1a, such electron/ion transport channels inside SLA are likely to facilitate three-dimensional homogeneous Zn^{2+} flux and enable Zn plating to take place within the entire anode with dendrite-free deposition. By contrast, the Zn plating/stripping occurs mainly on the two-dimensional surface of solid Zn foil and Zn powder anode, resulting in rampant dendrite evolution.[10]

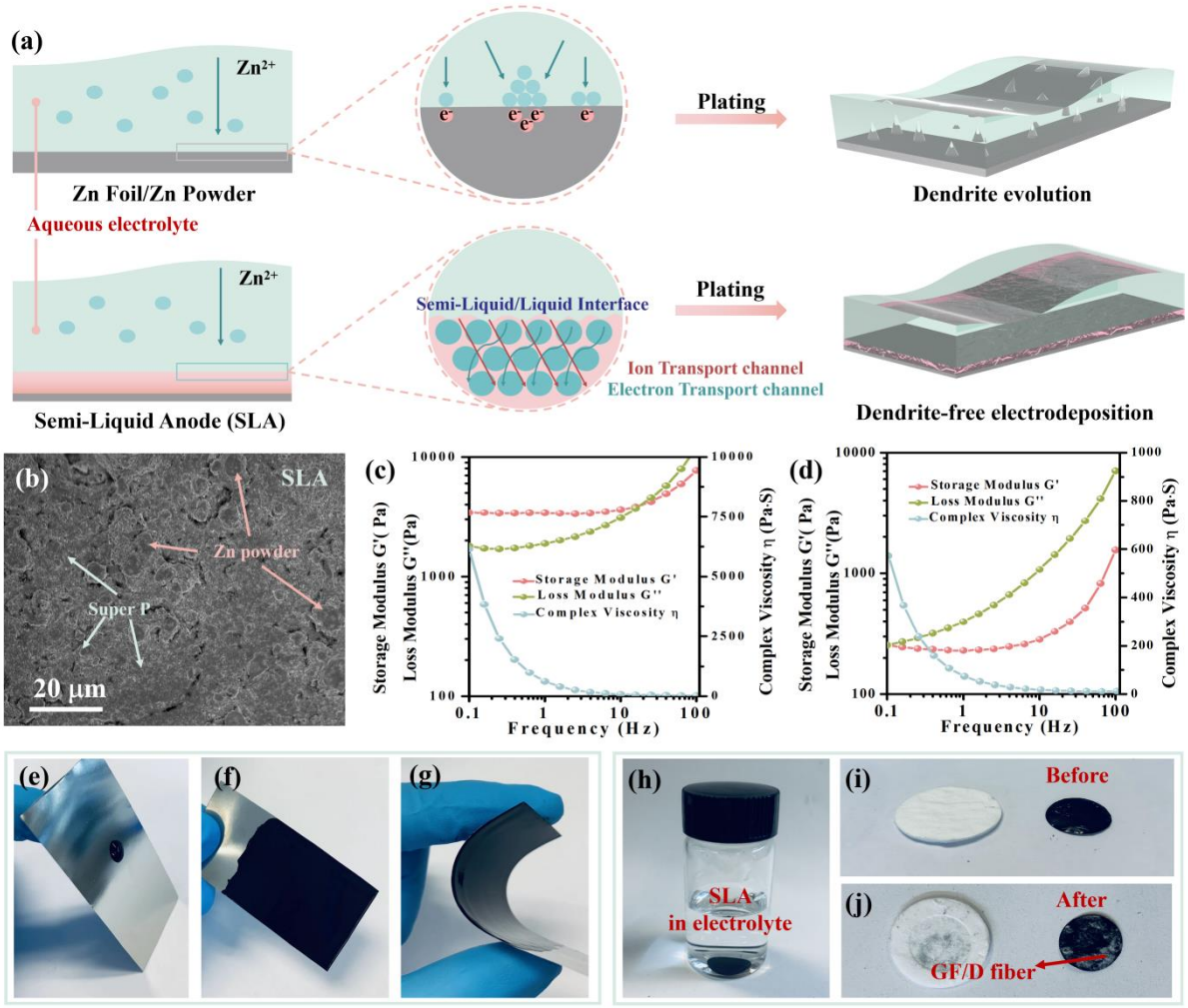

Figure 1. Essential characteristics of SLA. (a) Schematic illustrations of morphology evolution of SLA and Zn foil/Zn powder anodes; (b) SEM images of SLA; Rheological property of SLA under (c) 1% strain and (d) 10% strain; Digital images of (e) SLA adhered on stainless steel, and SLA coated on (f) flat and (g) curved stainless steel; (h) SLA immersed into 2 M $Zn(ClO_4)_2$ electrolyte; Status of SLA and separator (i) before and (j) after cycling in CR2032 cell.

The microstructure of SLA is characterized by a scanning electron microscope (SEM) and optical microscope. As shown in **Figures 1b and S5a,** all components are homogeneously mixed, thus forming a three-dimensional conductive network within the electrode. Moreover, **Figure S5b** demonstrates the cross-sectional optical image of SLA with the thickness about 70 μm. The mass loading of Zn in SLA is nearly 20 mg cm^{-2} (~16 mAh cm^{-2}), satisfying the areal capacity requirement for practical application. As the thickening agent, PEG in SLA can significantly tune the rheological property for stress relaxation during Zn plating. Rheometer was employed to assess the rheological property of the SLA. As depicted in **Figure 1c,** the storage modulus, loss modulus, and viscosity with respect to the frequency from 0.1 Hz to 100 Hz were recorded at room temperature. With the increase of frequency, the decreased complex viscosity indicates a typical non-Newtonian shear-thinning behavior. Meanwhile, the loss modulus becomes higher than the storage modulus as frequency increases, implying a transition from solid to liquid. Additionally, much lower viscosity and a liquid response throughout the entire frequency sweep can be observed under the shear strain of 10 % (**Figure 1d**). Owing to the unique rheological feature, the prepared SLA exhibits high viscosity, which can be firmly adhered to vertically tilted stainless steel without flow down **(Figure 1e)**. Under external force, SLA is easily coated on the current collector by a blade coating method and maintains stability under deformation, as demonstrated in **Figure 1f-g**.

To further examine the stability of the SLA electrode, it was gently soaked in the excessive electrolyte for 3 days. It is a delight to find that there is no apparent collapse of the SLA electrode, a reflection of the stability (**Figure 1h**). During the battery assembly, an "O" ring was inserted between SLA and GF/D film to provide enough space and confine the fluid electrode (**Figure S6**). The status of SLA before and after cycling for 10 h was displayed in **Figure 1h-j.** After removing the separator gently, the integrity of the SLA can be maintained, although some glass fibers are attached to the SLA. To evaluate whether the PEG will be

dissolved in the electrolyte during working conditions, we collected the Raman spectra of the electrolyte before and after 50 h cycling (**Figure S7**). As a reference, the Raman signal of 2 M $Zn(ClO_4)_2$ electrolyte containing 5vol.%, 10%, and 30% PEG additive were also recorded. The introduction of PEG leads to the presence of C-H bonds located at around 2947 cm^{-1}. The peak intensity becomes stronger with the increase in PEG amount. Note that the total amount of electrolyte is 20 μL, and the amount of PEG in SLA is about 18-24 μL. The dissolution of PEG would lead to up to 50 vol.% PEG in the electrolyte. In contrast, an extremely weak PEG signal is detected, suggesting the PEG dissolution is negligible and it can be well maintained in the SLA. These conclusions indicate the potential suitability of SLA as an anode for Zn-ion batteries.

The corrosion-resistance feature of the SLA anode is disclosed by electrochemical measurements. As illustrated in **Figure 2a**, Zn powder is wrapped by a PEG network, which could confine water molecules by forming hydrogen bonds.[11] With less contact with free H_2O molecules, Zn powder is effectively protected in the aqueous electrolyte solution. The electrochemical windows of various anodes are evaluated in **Figure 2b** to examine their stability. Compared to Zn foil and Zn powder anode, the hydrogen evolution and oxygen evolution reactions of SLA are all retarded. Identical consequences are also obtained in the linear polarization tests (**Figure S8)**. Briefly, a lower corrosion current of SLA can be observed than that of Zn foil and Zn powder anode, indicating a reduced corrosion tendency that prevents parasitic side reactions.[12] Furthermore, after repeated stripping and plating for 100 h, SLA maintains the erosion resistance with no byproducts detected in the XRD pattern (**Figure S9**).

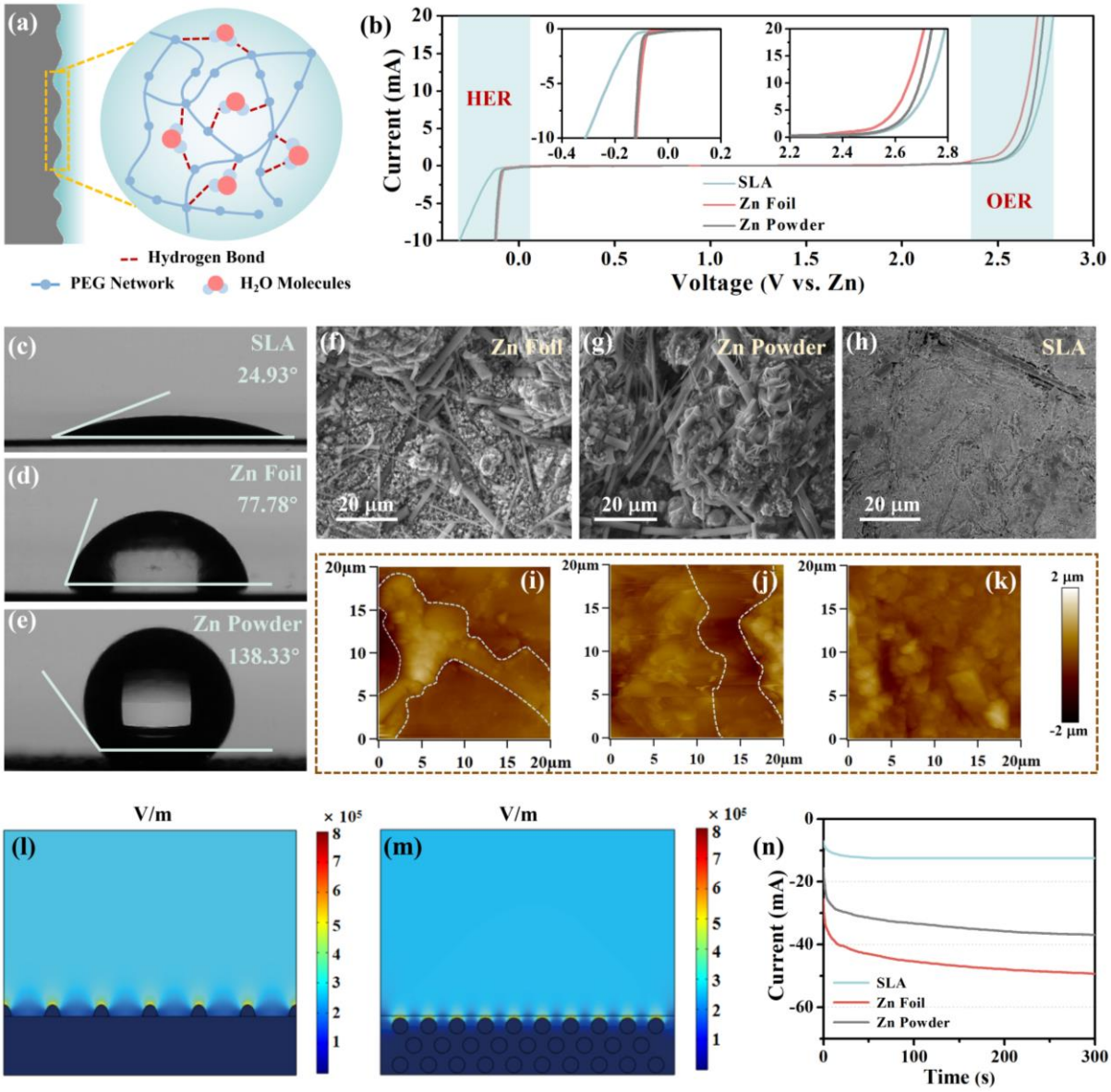

Figure 2. Corrosion resistance and deposition behavior of SLA. (a) Illustration of the formation of hydrogen bond; (b) Electrochemical window of various Zn anodes; Contact angle of (c) SLA, (d) Zn foil, and (e) Zn powder in the presence of 2 M $Zn(ClO_4)_2$ electrolyte; Morphology evolution of (f) Zn foil, (g) Zn powder and (h) SLA after plating at 5 mA cm^{-2} for 60 min and (i-k) corresponding AFM images; Electric field simulation of (l) solid Zn anode with protrusions on the surface and (m) SLA anode; (n) dI/dt curves for symmetric cell with various anodes under a constant voltage of -200 mV.

Turning to the deposition behavior, the contact angle was first recorded to quantify the effects of various anodes on wettability since it has a direct influence on Zn nucleation and

morphology evolution.[13] Notably, the SLA anode displays the static contact angle of 24.9° in 2 M $Zn(ClO_4)_2$ electrolyte due to a compatible semi-liquid/liquid interface (**Figure 2c**). By contrast, because of the hydrophobic nature, Zn foil and Zn powder anode exhibit much higher contact angles of 77.9° and 138.3°, respectively (**Figure 2d-e**). Such inferior hydrophilicity will aggravate depleted Zn^{2+} concentration and local electric field intensity, leading to rough Zn plating and rampant dendrites growth.[14] As a validation, the morphology evolution is examined by assembling symmetric cells with various Zn anodes. When a challenging current density of 5 mA cm^{-2} is adopted, aggravated dendrite initiation can be observed after 60 min deposition on the solid surface of Zn foil and Zn powder anode because of the "tip effect", i.e., under an electric field, the tip with large curvature on the surface of the object displays concentrated charge density and high electric field intensity, resulting in the occurrence of partial discharge (**Figure 2f-g**).[15] Apparent bulges can be observed on the surface of Zn foil and solid Zn powder anode (**Figure S10**). In sharp contrast, a much flat and smooth surface is maintained on the surface of SLA after plating (**Figure 2h**), consistent with improved electrochemical corrosion and wettability results.

An atomic force microscope (AFM) is adopted to further investigate the surface status of the cycled electrodes. Irregular and randomly distributed bulges and pits on the surface of Zn foil and Zn powder anode increase the risk of battery failure (**Figure 2i-j**). In contrast, the surface of SLA displays an improved surface status with uniform granules (**Figure 2k**). The distinct Zn growth behavior is revealed by electric field simulation. As shown in **Figure 2l**, surface protuberance sites with enhanced field intensity would result in the preferential growth of Zn and promote dendrite formation.[16] Encouragingly, the electric field distribution is notably homogeneous for the SLA anode. Although there are still partial areas with a concentrated electric field, the dendrite growth can be avoided due to the rheological property, thus realizing a flat and even deposition on the surface and inside (**Figure 2m**). To corroborate

the theoretical results, I (current)-t (time) test, which can sensitively reflect the surface change, are collected under an overpotential of -200 mV.[17] As for SLA, the alteration of dI/dt at the initial 70 s corresponds to the Zn nucleation and remains constant afterward, indicating a steady diffusion (**Figure 2n**). By contrast, a continuously changing current of Zn foil and Zn powder anode beyond 300 s proves a random diffusion, a driving force of frantic dendrite growth.[18] It is noteworthy that all samples exhibit a reduced interfacial resistance after I-t test, as shown **Figure S11**. The underlying reason is that the in-situ generated Cl^- conducting layer during the plating is conducive to the transportation of Zn ions.[19] The XPS spectrum and elemental mapping results after Zn deposition are provided to prove the presence of Cl-. As shown in **Figure S12**, the distributed elemental Cl can be observed on the surface of Zn, which agrees with the XPS results. Specifically, the corresponding Cl 2p XPS is fitted into the characteristic $2p_{3/2}$ and $2p_{1/2}$ splitting of Cl^- at 198.9 and 200.7 eV, respectively, owing to the reduction of ClO_4^- (**Figure S13**). The Zn^{2+} transference number of Zn foil-based cells is 0.42, increasing to 0.59 and 0.51 for cells with Zn powder and SLA, which are the typical values supporting fast Zn^{2+} transfer.[20]

To further elucidate the positive effect of the SLA on electrochemical performance, symmetric cells are assembled with 2 M $Zn(ClO_4)_2$ electrolytes. As shown in **Figure 3a**, SLA holds a stable voltage curve and long lifespan of more than 480 h at the current density of 2 mA cm^{-2} with a capacity of 2 mAh cm^{-2}. By contrast, a sudden and irreversible short circuit occurs in Zn foil because of the Zn dendrite growth and accumulation (~120 h), while the Zn powder anode suffers from even more rapid deterioration with abnormal electrochemical behavior in merely ~60 h. When increasing the deposition current density, the stress produced in the electrode becomes more significant, leading to more severe non-uniform Zn deposition on Zn foil and Zn powder anode.[21] However, the stress-release mechanism endows the SLA anode with resistance to dendrite growth. Therefore, the performance gap becomes much more prominent when the rate and capacity increase to 5 mA cm^{-2} and 5 mAh cm^{-2} (**Figure 3b**).

Briefly, SLA and Zn foil anode deliver a cycling lifespan of 450 h and 50 h, respectively. For Zn powder anode, the voltage jumps to over 500 mV at the initial stage and vibrates irregularly in the following cycles, indicating its unavailability under harsh conditions. Moreover, the rate performance of cells with different anodes is also studied at various current densities and capacities from 1 mA cm^{-2}/1 mAh cm^{-2} to 10 mA cm^{-2}/10 mAh cm^{-2}, as demonstrated in **Figure 3c**. Clearly, SLA exhibits a steady voltage profile in response to current densities and capacity changes. In contrast, the Zn foil and Zn powder anode encounter a sudden decay during increasing current rates. The morphology changes during repeat cycling are compared at 5 mA cm^{-2}. SEM image of the cycled Zn foil and Zn powder anode after failure exhibits a rough surface with dendrite distribution (**Figure S14**), while SLA retains a smooth morphology without the risk of piercing the separator by dendrites (**Figure 3d**). Impressively, when the condition of 10 mA cm^{-2} is applied, SLA can still work for over 250 h and 100 h under the capacity of 1 mAh cm^{-2} and 10 mAh cm^{-2} (**Figure S15**), realizing the high-power and high-capacity feature. Furthermore, SLA enables a stable plating/stripping for over 1600 h under a low temperature of -25 ℃ (**Figure S16**). Even under 2 mA cm^{-2}/2mAh cm^{-2}, a lifespan of over 110 h can be achieved (**Figure S17**). It is attributed to the fact that PEG and isolated ClO_4^- anion can form hydrogen bonds with H_2O molecules, significantly reducing the freezing point of electrolytes and the number of free water molecules.[22] Besides, the low temperature could partly suppress the side reactions (**Figure S18**).[23]

We note that PEG has also been widely adopted as an electrolyte additive. To show the different roles between electrolyte additives and thickening agent, the cycling stability of symmetric Zn powder//Zn powder cells employing 2 M $Zn(ClO_4)_2$ with various PEG additives (10 vol.%, 30 vol.%, and 50vol.%) are examined. As shown in **Figure S19**, the performance of Zn powder anode can only be operated with no more than 20 cycles at 5 mA cm^{-2}/5 mAh cm^{-2} and 10 mA cm^{-2}/10 mAh cm^{-2} regardless of PEG additive amounts. The inferior results indicate

that PEG plays a role other than electrolyte additive in SLA. Instead, the major role of PEG is to maintain the semi-liquid state of the electrode as a thickening agent to effectively release stress.[24]

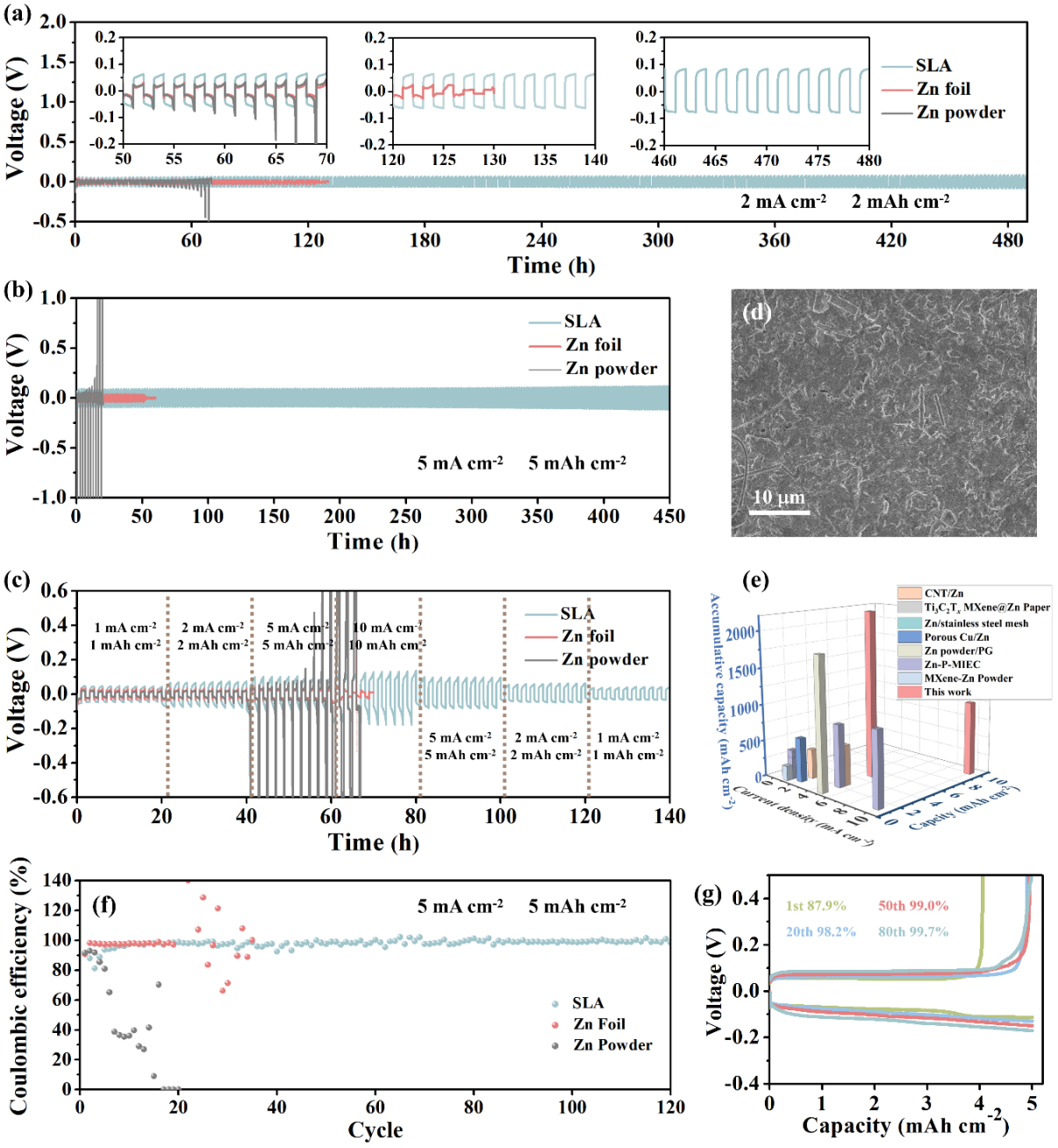

Figure 3. Cyclic performance and reversibility of SLA. Voltage profiles of symmetric cell based on SLA at (a) 2 mA cm^{-2}/2 mAh cm^{-2} and (b) 5 mA cm^{-2}/5 mAh cm^{-2}; (c) Rate performance from 1 mA cm^{-2}/1 mAh cm^{-2} to 10 mA cm^{-2}/10 mAh cm^{-2}; (d) SEM images of SLA anode after cycling for 100 h; (e) Performance comparison of SLA and other synthetic Zn anodes in terms

of current densities, specific capacities, and cumulative capacities; (f) Coulombic efficiency of symmetric cell with various Zn anodes at 5 mA cm^{-2} and (g) corresponding voltage profiles of Cu//SLA cell.

The performance of SLA-based symmetric cell is compared with other synthetic Zn anodes, including Mxene-Zn powder,[3a] CNT-Zn,[25] Zn powder/PG,[3b] Zn/stainless steel mesh,[26] porous Cu/Zn,[27] $Ti_3C_2T_x$ MXene@Zn Paper,[28] Zn-P-MIEC,[17] based on current density, specific capacity and cumulative capacity, as demonstrated in **Figure 3e** and **Table S1**. Most of the reported synthetic Zn anodes mainly focus on stability under relatively low current density and capacity. The reason may lie in profound dendrite growth under high rates. In contrast, because of the unique rheological property, anti-corrosive feature, and dual conducive medium of SLA, the electrochemical performance of SLA is significantly improved owing to the dendrite-free deposition. Specifically, an impressive cumulative capacity of 2250 mAh cm^{-2} and 1000 mAh cm^{-2} can be achieved at 5 mA cm^{-2} and 10 mA cm^{-2}, respectively.

Asymmetric cells employing Cu working electrodes and various Zn counter electrodes are assembled to evaluate the coulombic efficiency (CE) that is a decisive factor in assessing the reversibility and Zn utilization.[29] During the testing, a fixed amount of Zn is plated on Cu followed by charging to a cut-off voltage of 0.5 V. At the current density of 2 mA cm^{-2}, CE of asymmetric cells using Zn foil and Zn powder anode experience violent fluctuation with the average CE of less than 80% (**Figure S20a-c**), which may be attributed to the uneven Zn plating/stripping and reshaping of the surface.[30] On the contrary, the CE of the SLA-based cell gradually increases from 78.7% to 96.6% in the first 20 cycles and then remains stable with an average CE of about 98.2%, a reflection of improved reversibility. The smooth stripping/plating curves of Cu//SLA cell indicate uniform ion diffusion with continuous and steady electrochemical behavior (**Figure S20d**). Similarly, the Cu//SLA cell delivers a high average CE of 98.5% under 5 mA cm^{-2} as well as stable overpotential after a short activation process

(**Figure 3f-g**), outperforming the CE of cells with Zn foil and Zn powder anodes that deteriorate within 20 cycles (**Figure S21**). The CE values of Cu//SLA are one of the best among the Zn powder-based anodes (**Table S1**), attributing to the effect of the shear-thinning and side-reaction inhibition.

To probe the potential suitability of SLA in practical implementation, full cells are assembled coupling with a vanadium-based cathode, which is fabricated by a modified hydrothermal method.[1] The H_2O molecular and Cu^{2+} ion co-inserted V_2O_5 cathode (denoted as $Cu_xV_2O_5{\cdot}nH_2O$) displays porous morphology with Cu^{2+} distributed evenly (**Figure S22**). Moreover, the Cu^{2+} insertion can also be verified by XPS and XRD results, as analyzed in **Figure S23-S24**, in line with previous studies.[31] The cyclic voltammetry (CV) profile of the SLA-based cell is obtained at a scan rate of 0.5 mV s^{-1}, exhibiting two pairs of cathodic/anodic peaks associated with the Zn^{2+} insertion/extraction behavior (**Figure 4a**). Compared with the CV curves of Zn foil and Zn powder-based cells (**Figure S25)**, no side reactions are triggered, as proved by the similar redox peaks, indicating the compatibility of SLA with the cathode. The rate performance at various current densities from 0.5 to 10 A g^{-1} is illustrated in **Figure 4b.** The full cell based on SLA shows a high capacity of 378 mAh g^{-1} at 0.5 A g^{-1}. Even at 10 A g^{-1}, a high discharge capacity of over 180 mAh g^{-1} is realized, suggesting the superiority of SLA for Zn ion storage at high current densities. As for the long-term cycling test at 1 A g^{-1} (**Figure 4c**), a significant drop or fluctuation of the capacity and CE within 200 cycles is observed for cells using solid Zn powder and Zn foil anode. By contrast, the positive features of SLA endow the full cell with an impressive long-term cycling performance of more than 600 cycles with a capacity of 250 mAh g^{-1}. Impressively, the SLA-based full cell retains a capacity of nearly 120 mAh g^{-1} even after 5000 cycles at 10 A g^{-1}, superior to the contrast samples (**Figure 4d**). Benefiting from the anti-freezing properties, the performance of full cells with various anodes at 1 A g^{-1} under -25 ℃ is assessed in **Figure S26**. The SLA-based full cell maintains a high

capacity of 130 mAh g^{-1} after 500 cycles and shows improved capacity retention than the cells using Zn foil and Zn powder anode.

Furthermore, compared to Zn foil, the amount of granular zinc powder can be precisely controlled to improve the anode utilization. Based on this merit, SLA and Zn powder anode with a preset amount of Zn powder source are prepared to ensure the negative-to-positive (N:P) electrode capacity ratio of 5:1, followed by a cycling test under 1 A g^{-1} (**Figure S27**). A rapid capacity degradation is observed for Zn powder anode with no more than 30% capacity retained after 120 cycles. By contrast, the cell with SLA delivers a highly improved cycle stability within 120 cycles, accounting for over 80% of the highest capacity.

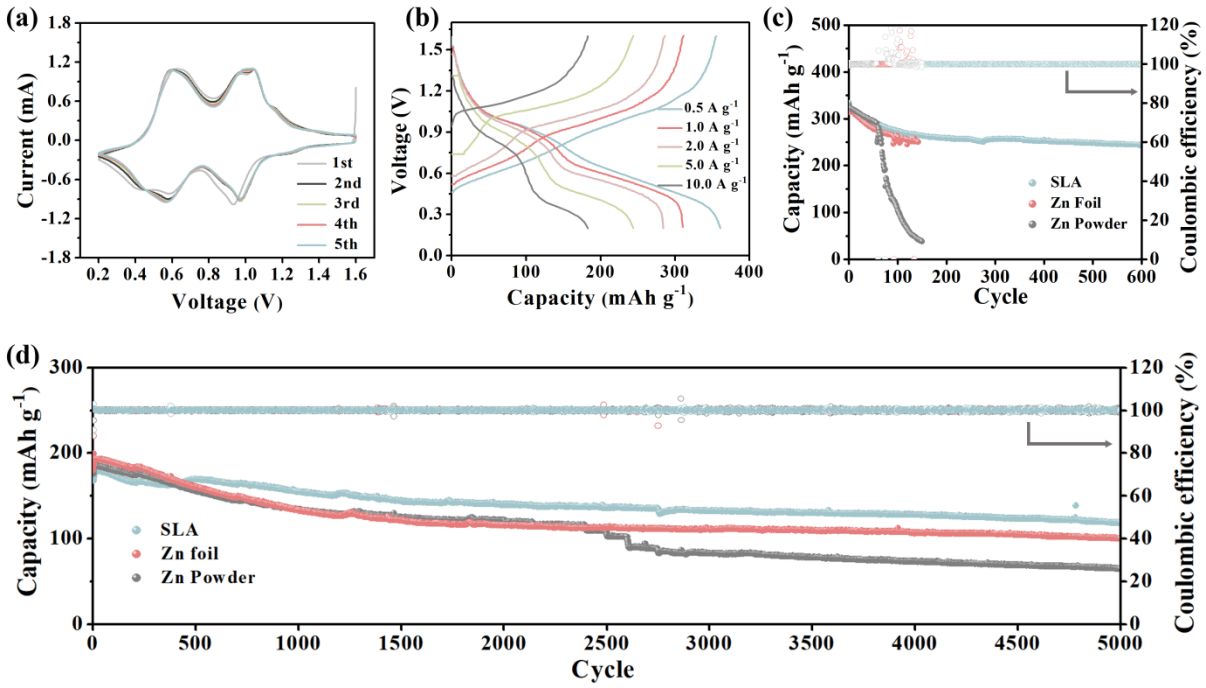

Figure 4. Full cell performance pairing with a vanadium-based cathode. (a) CV curves at a scan rate of 0.5 mV s^{-1}; (b) Voltage profiles at various current densities from 0.5-10 A g^{-1}; Cyclic performance at (c) 1 A g^{-1} and (d) 10 A g^{-1}.

Conclusion

In summary, a semi-liquid anode (SLA) with shear-thinning properties was designed to tackle dendrite and corrosion issues of Zn powder anodes by releasing stress and improving the electrochemical stability. In addition, electron/ion charge transfer occurs evenly across the entire anode, accompanied by homogeneous ion distribution and smooth deposition morphology. The symmetric cell enables significantly improved durability with a prolonged cycling life of 450 h at 5 mA cm^{-2} with the capacity of 5 mA cm^{-2}. Moreover, compared with the other reported Zn powder-based anodes, SLA shows an impressive cumulative capacity of more than 1000 mAh cm^{-2} under a high plating current density of 10 mA cm^{-2} and a capacity of 10 mAh cm^{-2}. Such an SLA anode also endows full cell with the long-term stability of over 5000 cycles pairing with a vanadium-based cathode. The presented methodology is expected to be further extended to other metal battery systems with powder active materials. Without complex chemical treatment, the simplicity of such anode synthesis makes it appealing for potential scale-up manufacturing.

Experimental procedures

Synthesis of SLA and solid Zn powder anode. In a typical procedure, zinc perchlorate hexahydrate was dissolved into poly(ethylene glycol) (MW=400) with a mass ratio of 1:2 by stirring for 1 h under 60 ℃. Subsequently, the transparent solution was mixed with a solid mixture containing commercial Zn powder/Super P (95:5 wt.%), and the solid/liquid ratio was controlled as 1 g/1 mL. After grinding for 2 h, the as-prepared stable suspension was cast into stainless steel and stood for 1 h to ensure close contact with the current collector, thus forming a stable SLA. As the control experiment, commercial Zn powder, Super P, and polyvinylidene difluoride (PVDF) with a mass ratio of 90:5:5 were mixed in a N-Methylpyrrolidone (NMP) solvent. The uniform slurry was then coated on stainless steel followed by drying under 80 ℃ for 24 h to obtain the solid Zn powder anode.

Synthesis of the vanadium-based cathode. Briefly, 365 mg V_2O_5, 2 mL H_2O_2 and 75 mg $Cu(NO_3)_2$ were added into 60 mL deionized water in sequence to obtain a homogeneous solution, which was then transferred into a 100 mL Teflon-lined autoclave for hydrothermal reaction under 120 ℃. After 12 h, the products were washed with ethanol for 3 times and vacuum-dried overnight under 80 ℃. Finally, Cu^{2+} and H_2O molecular co-inserted products were defined as $Cu_xV_2O_5{\cdot}nH_2O$. The cathode was prepared by mixing $Cu_xV_2O_5{\cdot}nH_2O$, Super P and PVDF in a weight ratio of 7:2:1 in NMP to form a homogeneous slurry, which was then cast on stainless steel and vacuum-dried at 80 ℃ overnight.

Materials Characterization, Electrochemical Test and Simulation, were detailed in Supporting Information.

Acknowledgments

This work was supported by the General Research Fund (GRF) scheme of the Hong Kong Research Grants Council (Project No. 15307221).

Reference

[1] a) D. Kundu, B. D. Adams, V. Duffort, S. H. Vajargah and L. F. Nazar, *Nat. Energy* **2016**, *1*, *16119;* b) Z. Hou, B. Zhang, *EcoMat* **2022**, e12265.

[2] a) V. Verma, S. Kumar, W. Manalastas and M. Srinivasan, *ACS Energy Lett.* **2021**, *6*, 1773; b) A. Naveed, A. Ali, T. Rasheed, X. Wang, P. Ye, X. Li, Y. Zhou, S. Mingru and Y. Liu, *J. Power Sources* **2022**, *525*, *231122*; c) L. E. Blanc, D. Kundu and L. F. Nazar, *Joule* **2020**, *4*, 771; d) A. Naveed, T. Rasheed, B. Raza, J. Chen, J. Yang, N. Yanna and J. Wang, *Energy Storage Mater.* **2022**, *44*, 206.

[3] a) X. Li, Q. Li, Y. Hou, Q. Yang, Z. Chen, Z. Huang, G. Liang, Y. Zhao, L. Ma, M. Li, Q. Huang and C. Zhi, *ACS Nano* **2021**, *15*, 14631; b) W. Du, S. Huang, Y. Zhang, M. Ye and C. C. Li, *Energy Storage Mater.* **2022**, *45*, 465.

[4] a) P. Xue, C. Guo, L. Li, H. Li, D. Luo, L. Tan and Z. Chen, *Adv. Mater.* **2022**, *34*, e2110047; b) Y. Hao, D. Feng, L. Hou, T. Li, Y. Jiao and P. Wu, *Adv. Sci.* **2022**, *9*, e2104832; c) Q. Liu, Y. Wang, X. Hong, R. Zhou, Z. Hou and B. Zhang, *Adv. Energy Mater.* **2022**, *12*, 2022318; d) J. Shin, J. Lee, Y. Kim, Y. Park, M. Kim and J. W. Choi, *Adv. Energy Mater.* **2021**, *11*, 2100676; e) L. Wang, W. Huang, W. Guo, Z. H. Guo, C. Chang, L. Gao and X. Pu, *Adv. Funct. Mater.* **2021**, *32*, 2108533; f) L. Cao, D. Li, T. Deng, Q. Li and C. Wang, *Angew. Chem. Int. Ed.* **2020**, *59*, 19292; g) J. Hao, L. Yuan, C. Ye, D. Chao, K. Davey, Z. Guo and S. Z. Qiao, *Angew. Chem. Int. Ed.* **2021**, *60*, 7366.

[5] Y. Ding, X. Guo, Y. Qian, L. Xue, A. Dolocan and G. Yu, *Adv. Mater.* **2020**, *32*, e2002577.

[6] X. Wang, W. Zeng, L. Hong, W. Xu, H. Yang, F. Wang, H. Duan, M. Tang and H. Jiang, *Nat. Energy* **2018**, *3*, 227.

[7] J. Gu, Y. Tao, H. Chen, Z. Cao, Y. Zhang, Z. Du, Y. Cui and S. Yang, *Adv. Energy Mater.* **2022**, *12*, 2200115.

[8] a) G. H. Lee, Y. R. Lee, H. Kim, D. A. Kwon, H. Kim, C. Yang, S. Q. Choi, S. Park, J. W. Jeong and S. Park, *Nat. Commun.* **2022**, *13*, 2643; b) K. Kalantar-Zadeh, J. Tang, T. Daeneke, A. P. O'Mullane, L. A. Stewart, J. Liu, C. Majidi, R. S. Ruoff, P. S. Weiss and M. D. Dickey, *ACS Nano* **2019**, *13*, 7388.

[9] a) S. Li, H. Wang, J. Cuthbert, T. Liu, J. F. Whitacre and K. Matyjaszewski, *Joule* **2019**, *3*, 1637; b) Y. Zhang, Z. Han, Z. Huang, C. Zhang, C. Luo, G. Zhou, W. Lv and Q.-H. Yang, *ACS Energy Lett.* **2021**, *6*, 3761.

[10] a) J. Y. Kim, G. Liu, R. E. A. Ardhi, J. Park, H. Kim and J. K. Lee, *Nano-Micro Lett.* **2022**, *14*, 46; b) X. Xie, S. Liang, J. Gao, S. Guo, J. Guo, C. Wang, G. Xu, X. Wu, G. Chen and J. Zhou, *Energy Environ. Sci.* **2020**, *13*, 503.

[11] a) J. Xie, Z. Liang and Y. C. Lu, *Nat. Mater.* **2020**, *19*, 1006; b) Z. Cao, X. Zhu, S. Gao, D. Xu, Z. Wang, Z. Ye, L. Wang, B. Chen, L. Li, M. Ye and J. Shen, *Small* **2022**, *18*, e2103345;

c) J. Zhou, H. Yuan, J. Li, W. Wei, Y. Li, J. Wang, L. Cheng, D. Zhang, Y. Ding, D. Chen and H. Wang, *Chem. Eng. J.* **2022**, *442*, 136218.

[12] a) Z. Hou, Z. Lu, Q. Chen and B. Zhang, *Energy Storage Mater.* **2021**, *42*, 517; b) D. Xie, Z. W. Wang, Z. Y. Gu, W. Y. Diao, F. Y. Tao, C. Liu, H. Z. Sun, X. L. Wu, J. W. Wang, J. P. Zhang, *Adv. Funct. Mater.* **2022**, 32, 2204066.

[13] S. H. Park, S. Y. Byeon, J.-H. Park and C. Kim, *ACS Energy Lett.* **2021**, *6*, 3078.

[14] a) P. Chen, X. Yuan, Y. Xia, Y. Zhang, L. Fu, L. Liu, N. Yu, Q. Huang, B. Wang, X. Hu, Y. Wu and T. van Ree, *Adv. Sci.* **2021**, *8*, e2100309; b) S. Liu, J. Mao, W. Pang, J. Vongsvivut, X. Zeng, L. Thomsen, Y. Wang, J. Liu, D. Li, Z. Guo, *Adv. Funct. Mater.* **2021**, 31, 2104281.

[15] P. Liu, B. Chen, C. Liang, W. Yao, Y. Cui, S. Hu, P. Zou, H. Zhang, H. J. Fan and C. Yang, *Adv. Mater.* **2021**, *33*, e2007377.

[16] N. Zhang, S. Huang, Z. Yuan, J. Zhu, Z. Zhao and Z. Niu, *Angew. Chem. Int. Ed.* **2021**, *60*, 2861.

[17] M. Zhang, P. Yu, K. Xiong, Y. Wang, Y. Liu and Y. Liang, *Adv. Mater.* **2022**, *34*, e2200860.

[18] T. Wang, C. Li, X. Xie, B. Lu, Z. He, S. Liang and J. Zhou, *ACS Nano* **2020**, *14*, 16321.

[19] a) X. Guo, Z. Zhang, J. Li, N. Luo, G.-L. Chai, T. S. Miller, F. Lai, P. Shearing, D. J. L. Brett, D. Han, Z. Weng, G. He and I. P. Parkin, *ACS Energy Lett.* **2021**, *6*, 395; b) L. Wang, Y. Zhang, H. Hu, H. Y. Shi, Y. Song, D. Guo, X. X. Liu and X. Sun, *ACS Appl. Mater. Interfaces* **2019**, *11*, 42000.

[20] a) J. Cong, X. Shen, Z. Wen, X. Wang, L. Peng, J. Zeng, J. Zhao, Energy Storage Mater. 2021, 35, 586; b) J. Hu, Y. Qu, F. Shi, J. Wang, X. He, S. Liao, L. Duan, Adv. Funct. Mater. 2022, 2209463.

[21] a) J. H. Cho, X. Xiao, K. Guo, Y. Liu, H. Gao and B. W. Sheldon, *Energy Storage Mater.* **2020**, *24*, 281; b) J. Hu, Z. Sun, Y. Gao, P. Li, Y. Wu, S. Chen, R. Wang, N. Li, W. Yang, Y. Shen and S.-H. Bo, *Cell Rep. Phy. Sci.* **2022**, *3*, 100938.

[22] a) S. Huang, L. Hou, T. Li, Y. Jiao and P. Wu, *Adv. Mater.* **2022**, *34*, e2110140; b) Y. Sun, H. Ma, X. Zhang, B. Liu, L. Liu, X. Zhang, J. Feng, Q. Zhang, Y. Ding, B. Yang, L. Qu and X. Yan, *Adv. Funct. Mater.* **2021**, *31*, 2101277.

[23] C. Yan, Y. Wang, X. Deng, Y. Xu, Nano-Micro Lett. 2022, 14, 98.

[24] a) Y. Wu, Z. Zhu, D. Shen, L. Chen, T. Song, T. Kang, Z. Tong, Y. Tang, H. Wang and C. S. Lee, Energy Storage Mater. 2022, 45, 1084; b) Z. Cao, X. Zhu, S. Gao, D. Xu, Z. Wang, Z. Ye, L. Wang, B. Chen, L. Li, M. Ye, and J. Shen, Small 2022, 18, 2103345; b) A. Mitha, A. Z. Yazdi, M. Ahmed and P. Chen, ChemElectroChem, 2018, 5, 2409.

[25] Y. Zeng, X. Zhang, R. Qin, X. Liu, P. Fang, D. Zheng, Y. Tong and X. Lu, *Adv. Mater.* **2019**, *31*, e1903675.

[26] J. Zhao, H. Ren, Q. Liang, D. Yuan, S. Xi, C. Wu, W. Manalastas, J. Ma, W. Fang, Y. Zheng, C.-F. Du, M. Srinivasan and Q. Yan, *Nano Energy* **2019**, *62*, 94.

[27] X. Shi, G. Xu, S. Liang, C. Li, S. Guo, X. Xie, X. Ma and J. Zhou, *ACS Sustain. Chem. Eng.* **2019**, *7*, 17737.

[28] Y. Tian, Y. An, C. Wei, B. Xi, S. Xiong, J. Feng and Y. Qian, *ACS Nano* **2019**, *13*, 11676.

[29] C. Li, A. Shyamsunder, A. G. Hoane, D. M. Long, C. Y. Kwok, P. G. Kotula, K. R. Zavadil, A. A. Gewirth and L. F. Nazar, *Joule* **2022**, *6*, 1103.

[30] S. Zhou, Y. Wang, H. Lu, Y. Zhang, C. Fu, I. Usman, Z. Liu, M. Feng, G. Fang, X. Cao, S. Liang and A. Pan, *Adv. Funct. Mater.* **2021**, *31*, 2104361.

[31] a) Y. Yang, Y. Tang, G. Fang, L. Shan, J. Guo, W. Zhang, C. Wang, L. Wang, J. Zhou and S. Liang, *Energy Environ. Sci.* **2018**, *11*, 3157; b) H. Wang, X. Bi, Y. Bai, C. Wu, S. Gu, S. Chen, F. Wu, K. Amine and J. Lu, *Adv. Energy Mater.* **2017**, *7*, 1602720.